Published in final edited form as:
J Am Chem Soc. 2018 May 23; 140(20): 6374–6382. doi:10.1021/jacs.8b02603.

An *S* = 1/2 Iron Complex Featuring N_2, Thiolate, and Hydride Ligands: Reductive Elimination of H_2 and Relevant Thermochemical Fe–H Parameters

Nina X. Gu, **Paul H. Oyala**, and **Jonas C. Peters***
Division of Chemistry and Chemical Engineering, California Institute of Technology, Pasadena, California 91125, United States

Abstract

Believed to accumulate on the Fe sites of the FeMo-cofactor (FeMoco) of MoFe-nitrogenase under turnover, strongly donating hydrides have been proposed to facilitate N_2 binding to Fe and may also participate in the hydrogen evolution process concomitant to nitrogen fixation. Here, we report the synthesis and characterization of a thiolate-coordinated $Fe^{III}(H)$-(N_2) complex, which releases H_2 upon warming to yield an Fe^{II}–N_2–Fe^{II} complex. Bimolecular reductive elimination of H_2 from metal hydrides is pertinent to the hydrogen evolution processes of both enzymes and electrocatalysts, but well-defined examples are uncommon and usually observed from diamagnetic second-and third-row transition metals. Kinetic data obtained on the HER of this ferric hydride species are consistent with a bimolecular reductive elimination pathway, arising from cleavage of the Fe–H bond with a computationally determined BDFE of 55.6 kcal/mol.

Graphical Absrtact

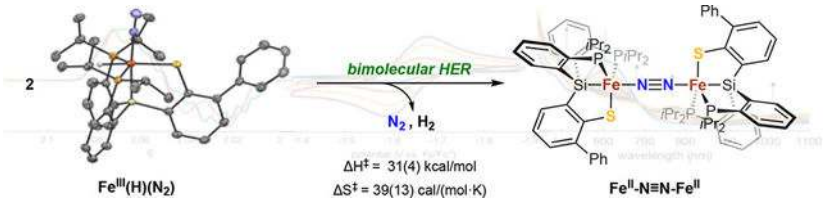

INTRODUCTION

Despite a wealth of recent progress toward functional models of biological N_2-to-NH_3 conversion,[1,2] many questions remain as to how the active-site cofactors of nitrogenase enzymes, as in the iron–molybdenum cofactor (FeMoco) of MoFe-nitrogenase,[3] manage N_2 binding and the subsequent bond-breaking and making steps en route to NH_3 formation.

*Corresponding Author: jpeters@caltech.edu.

Supporting Information
The Supporting Information is available free of charge on the ACS Publications website at DOI:10.1021/jacs.8b02603.
Experimental procedures and compound characterization data (PDF)
X-ray data (CIF)
Cartesian coordinates (MOL)

The authors declare no competing financial interest.

While the community has primarily focused on iron as the most likely site(s) of N_2 binding in recent years,[4] a particular conundrum concerns the presence of relatively weak-field sulfide (S^{2-}) ligands around the candidate iron sites,[5] as yet unknown ligands in Fe–N_2 model chemistry, and the related requirement that N_2 binding must occur at a biologically accessible redox potential.[6]

One plausible scenario to help account for N_2 binding at iron at the FeMoco is that redox leveling of successive electron-transfer steps may be achieved by concomitant proton transfers[7] to generate, for example, protonated sulfides (e.g., SH^-)[8] and/or iron hydrides (e.g., Fe–H, Fe–(μ-H)–Fe).[9] Such a scenario would not only alleviate local charge build-up, thereby buffering redox potential, but would also install comparatively strong-field hydrides that are compatible with, and might even facilitate, Fe(N_2)-bound states.[4,10] Hence, there is substantial motivation to prepare synthetic model complexes featuring Fe–N_2 with a combination of thioether[11,12]/thiolate[13,14] and hydride ligands within the immediate iron coordination sphere.[15]

Relatedly, spin-active model complexes of these types, $S = 1/2$ systems especially, may provide needed spectroscopic parameters to help guide reliable assignments of intermediate states within the biological systems. Accordingly, various EPR techniques have proven effective for observing $S = 1/2$ intermediate states during nitrogenase turnover (e.g., hydride and N_xH_y-bound states),[4,9,16] and an EPR-active, hydride-bound nitrogenase state, where the hydride ligands have been assigned as iron-ligated, has been proposed to undergo H_2 elimination concurrent with nitrogen uptake and subsequent reduction.[9a,17]

H_2 elimination steps from metal-bound hydride states are also presumed to be relevant to iron-rich hydrogenase enzymes[18,19] and often in synthetic molecular catalysts for the hydrogen evolution reaction (HER),[19,20] including examples featuring Fe, Co, and Ni.[20b,20C,21,22] When considering the key H–H bond formation step from metal hydride complexes, there are a number of pathways one might consider, including bond formation via direct protonation of the hydride ligand,[23] ligand-facilitated protonation of metal hydrides,[20b,24] and reductive elimination from a metal polyhydride species.[25] In particular, although bimolecular reductive elimination of H_2 from metal hydride species has been demonstrated to play a role in electrocatalytic systems for proton reduction,[22] examples of such reactivity from well-defined terminal metal hydride complexes are limited.[26] There is thus substantial motivation to map the reactivity patterns and fundamental thermochemical parameters of Fe–H (and other M–H) species in the presence of thiolate and N_2 ligands, particularly in systems where H_2 evolution is viable.

In this study, we report the synthesis and characterization of structurally unusual Fe(H)(N_2)(thiolate) complexes in two redox states, $S = 0$ Fe^{II}(H)(N_2)(thiolate) and $S = 1/2$ Fe^{III}(H)(N_2)(thiolate), which have each been characterized by numerous techniques, including by XRD analysis and pulse electron–nuclear double resonance (ENDOR) spectroscopy for the $S = 1/2$ state. EPR data for terminally bound and open-shell Fe–H species, regardless of the other ligands in the coordination sphere, are highly limited.[2,27,28] Furthermore, prior to this report, Fe–N_2 complexes have, to our knowledge, only been characterized in oxidation states

of 2+ and lower;[29] our finding that Fe(III) binds a weakly activated N_2 ligand in the presence of thiolate and hydride ligands is hence noteworthy.

The $Fe^{III}(H)(N_2)$(thiolate) species persists at low temperatures in solution but undergoes bimolecular conversion to a diiron $Fe^{II}–N_2–Fe^{II}$ product upon warming, along with associated loss of H_2. Such reactivity has strong precedence for second-and third-row transition metal hydrides[26] but is still unusual among first-row metal hydrides[30–34] and among paramagnetic hydrides in general.[26a,26b,27] Thus, the present Fe^{II}/Fe^{III} hydride system offers an opportunity to map kinetic parameters for H_2 evolution and fundamental Fe–H thermochemical (H^+, $H^•$, H^-) parameters of broad current interest in the context of HER and small-molecule reduction catalysis.[35]

RESULTS AND DISCUSSION

Synthesis and Characterization of $Fe^{II}(H)(N_2)$(thiolate), 7-H, and $Fe^{III}(H)(N_2)$(thiolate), 8-H.

To template a thiolate-supported iron(N_2) complex, we envisioned the incorporation of a thiolate group within a polyphosphino silyl framework, a motif our laboratory has previously utilized to gain entry into Fe(N_2) chemistry (Scheme 1).[36] Alkylation of 2-phenylbenzenethiol (**1**)[37] followed by directed ortho lithiation provides the aryllithium salt (**3**) as a TMEDA adduct (88%). Treatment of bis(*o*-diisopropylphosphinophenyl)chlorosilane (**4**)[12] with **3** affords the ligand $HSiP_2S$ (**5**) (Scheme 1a; 66%). A singlet corresponding to the two phosphines is observed by ^{31}P NMR spectroscopy at 1.10 ppm, and IR spectroscopy reveals an Si–H stretch at 2228 cm^{-1}. Complexation of **5** using $FeCl_2$ and subsequent addition of excess MeMgCl promotes cleavage of the Si–H and S–*i*Pr bonds to afford the thiolate-bound, yellow-brown complex $[(SiP_2S)\text{-}Fe]_2(\mu\text{-}N_2)$ (**6**) in moderate yield (Scheme 1b). The two previous reports of thiolate-coordinated Fe(N_2) species exhibit terminally bound N_2 ligands.[13,14]

Compound **6** exhibits a bridging N_2 ligand coordinated end on to each iron center. This is confirmed by X-ray crystallography, which elucidates two similar but crystallo-graphically distinct iron centers in the solid state with a bridging N≡N bond length of 1.138(2) Å (Figure 1a, Table 1). A weak N_2 stretch at 1888 cm^{-1} is observed in the solid-state by IR spectroscopy, consistent with the absence of a rigorous inversion center. The 80 K ^{57}Fe Mössbauer spectrum of **6** can be fit to one unique iron center ($\delta = 0.447$ mm/s, $\Delta E_Q = 1.776$ mm/s) with an isomer shift similar to other five-coordinate, $S = 1$ iron species ligated by related polyphosphine ligands.[38] The room-temperature solution-state magnetic moment of compound **6** ($\mu_{eff} = 4.8\ \mu_B$) suggests an overall $S = 2$ species, and magnetic susceptibility data collected between 25 °C and −75 °C obey the Curie–Weiss law. These data are consistent with a description for 6 featuring two $S = 1$ centers with strong ferromagnetic exchange. Strong ferromagnetic coupling has been observed in an $S = 3/2$, dinitrogen-bridged Fe(I)/Fe(II) species,[12] and weak ferromagnetic exchange in an $S = 3$ Fe(I)/Fe(II) species,[39] both previously described by our laboratory. Fe–N≡N–Fe species are also known that exhibit antiferromagnetic coupling between iron centers[2] or bear iron centers antiferromagnetically coupled to an $S = 1$ dinitrogen (N_2^{2-}) unit.[40]

To install the desired hydride ligand on iron, we found that treatment of diiron **6** with lithium triethylborohydride affords red, diamagnetic $[(SiP_2S)Fe^{II}(H)(N_2)]Li(THF)_2$ (**7-H**). X-ray diffraction data confirms the assignment of 7-H and reveals a coordinated dinitrogen with an N–N bond length of 1.128(9)Å. Although the hydride ligand could not be resolved from the XRD analysis of **7-H**, a wide P–Fe–P angle of 145.24(7)° is consistent with the presence of a hydride located between the two phosphine ligands. Furthermore, a hydridic resonance coupled to the two 31P nuclei is observed by 1H NMR spectroscopy at −19.32 ppm (t, $^3J_{H,P}$ = 71.3 Hz), absent in the ^{1}H NMR spectrum of $[(SiP_2S)Fe^{II}(D)(N_2)]Li(THF)_2$ (**7-D**); the latter species is obtained in an analogous fashion to **7-H** with lithium triethylborodeuteride. IR spectroscopy of compound **7-H** reveals three N_2 stretches (2020, 1976, 1935 cm^{-1}) that presumably arise from distinct coordination modes of the lithium cation[41] and an Fe–H stretch at 1864 cm^{-1} that is absent in the IR spectrum of **7-D**. Treatment of **7-H** with 12-crown-4 affords $[(SiP_2S)Fe^{II}(H)(N_2)][Li(12\text{-crown-4})(THF)]$ (**7-H**(**crown**)), which is isolated as a red solid. IR spectroscopy of **7-H**(**crown**) shows a single N_2 stretch at 1971 cm^{-1} (ν(Fe– H) at 1886 cm^{-1}), and XRD analysis of **7-H**(**crown**) confirms its relation to **7-H** (Figure 1b, Table 1).

Room-temperature cyclic voltammetry measurements of **7-H** in THF reveal a reversible oxidation event at −1.63 V vs Fc/Fc^+, corresponding to the $Fe^{III/II}$ couple (Figure 2a). Chemical oxidation of the Fe(II) precursor **7-H** with $[Cp_2Co][PF_6]$ affords a dark blue solution that persists for several hours at room temperature, enabling the characterization of the title complex $(SiP_2S)Fe^{III}(H)(N_2)$ (**8-H**). Neutral 8-H cocrystallizes with crystals of the cobaltocene byproduct; despite repeated attempts, **8-H** and Cp_2Co could not be separated, owing to very similar solubility. Nevertheless, high quality X-ray data confirms the solid-state structure of **8-H** (Figure 1, Table 1).

Compared to the crystallographic data for **7-H**(**crown**), the structure of **8-H** reveals elongation of the Fe–N bond (from 1.810(4) to 1.882(3) Å) and contraction of the N≡N bond (1.117(6) to 1.077(4) Å) upon oxidation, consistent with poorer π-donicity from the more oxidized iron center. The crystallographically determined N≡N bond length of **8-H** of 1.077(4) Å is close to the bond length of free N_2 (1.0975).[42] Furthermore, the Fe–P bond lengths elongate upon conversion of diamagnetic **7-H**(**crown**) to doublet **8-H**, consistent with the observed correlation between spin state and Fe–P bond length noted on related polyphosphino Fe complexes.[43] The hydride ligand can be located in the difference map of **8-H** and freely refined to an Fe–H bond length of 1.54(4) Å, comparable to the crystallographically determined Fe–H bond lengths of other paramagnetic, terminal iron hydride species.[28a,28b] The isotopologue $(SiP_2S)Fe^{III}(D)(N_2)$ (**8-D**) is prepared in an analogous fashion to **8-H** via oxidation of **7-D**. Spectroscopic characterization of charge-neutral **8-H** and **8-D** is carried out on samples generated in situ at −78 °C. Furthermore, manipulations with **8-H** and **8-D** are carried out at low temperature due to their thermal instability (vide infra).

The IR spectrum of 8-**H** reveals N_2 and Fe–H stretches at 2123 and 1852 cm^{-1}, respectively (Figure 2b). Compared to **7-H**(**crown**), there is a 152 cm^{-1} shift in the N_2 stretching frequency upon oxidation, consistent with a metal-centered oxidation. The observed Fe-D IR

stretch of **8-D** is in good agreement with the values predicted by the simple harmonic oscillator model (calculated: 1321 cm^{-1}; observed: 1333 cm^{-1}). Additionally, the ^{57}Fe Mössbauer spectrum of **8-H** is consistent with a single iron-containing species ($\delta = 0.227$ mm/s, $\Delta E_Q = 1.734$ mm/s); these parameters correspond to an approximate fit due to asymmetric line broadening of the spectrum (Figure 2c).[44] Broad, paramagnetically shifted peaks are observed by ^1H NMR spectroscopy of **8-H** at −78 °C, and the $S = 1/2$ spin state is corroborated by continuous-wave (CW) EPR spectroscopy (Figure 2d, vide infra).[45]

In addition to the coordination of a strong field hydride ligand, the ferric Fe–N_2 species **8-H** is additionally stabilized by partial spin delocalization onto the aryl thiolate ligand;[46] this attenuates the perturbation to Fe–N_2 and Fe–H bonding upon oxidation. There is significant contraction in the Fe–S bond of the more oxidized **8-H** (2.2185(7) Å) compared to **7-H(crown)** (2.339(2) Å), which contrasts with the observed elongation of the Fe–P bonds in the ferric analogue (Fe–P_{avg}:2.17 Å in **7-H(crown)**, 2.25 Å in **8-H**).

The spin density map of the gas-phase optimized **8-H** structure (M06-L: def2tzvp (Fe), def2svp (all other atoms))[47] indeed reveals partial spin leakage onto the sulfur atom, with lesser delocalization onto the other coordinated fragments (Figure 3). However, the calculated distribution of unpaired spin suggests the oxidation is predominantly metal based, which is consistent with the significant shift in N_2 stretching frequency observed between **7-H(crown)** and **8-H**. There is a calculated spin density of 0.92 e^- (58%) localized at Fe and 0.18 e^- (11%) at sulfur. Additionally, the calculated −0.029 e^- (2%) localized on the hydride fragment is consistent with the experimentally observed hyperfine coupling obtained via EPR and ENDOR spectroscopies (vide infra).

EPR and ENDOR Characterization of 8-H.

The 77 K X-band CW EPR spectrum of **8-H** (Figure 2d) shows a rhombic signal, which is simulated with slight g anisotropy (g = [2.07,2.0475, 2.02]). Q-band Davies ENDOR spectra collected at 18.5 K on **8-H** across the EPR envelope are simulated well (Figure 4a) with coupling to the hydridic ^1H nucleus ($A(^1H) = \pm$ [15, 56, 58] MHz) with a small Euler rotation $\beta = 25°$ of the ^1H A tensor relative to the g-tensor, and two similar but inequivalent ^{31}P nuclei ($A(^{31}P\alpha) = \pm$[31, 36, 27] MHz; $A(^{31}P\beta) = \pm$[28, 25, 23] MHz). Additional coupling to a ^1H nucleus is also observable ($A(^1H') = \pm$[6.8, 10, 6.8] MHz), likely arising from coupling to hydrogen atom(s) of the ligand; this coupling is also present in the spectra of **8-D**. ENDOR data on **8-D** are additionally simulated (Figure 4b) with coupling to two ^{31}P nuclei with identical parameters as that of **8-H** and a ^2H nucleus; almost complete disappearance of the 1H hydride signal is also evident. The ^2H signal can be suitably simulated by scaling $A(^1H)$ by the ratio of the $^2H/^1H$ gyromagnetic ratios, ($A(^2H) = \pm$[2.3, 8.6, 8.9] MHz), and the X-band CW EPR spectra of both **8-H** and **8-D** are simulated well by using the hyperfine coupling constants obtained via ENDOR spectroscopy (Figure 4c,d).

Pulse EPR data on an $S = 1/2$ freeze-trapped state of MoFe nitrogenase, which has been observed during FeMoco-catalyzed proton reduction[9] and nitrogen fixation,[48] are consistent with the accumulation of hydride intermediates at the cofactor under turnover conditions. Two ^1H nuclei (H_1: $a_{iso} = 24.3$ MHz, **T** = [−13.3, 0.7, 12.7] MHz; H_2: $a_{iso} = 22.3$ MHz, **T** =

[10.7, −12.3,1.7] MHz) are assigned as Fe−(μ-H)−Fe moieties.[9a] The ^{1}H signals are believed to arise from bridging, as opposed to terminal hydrides, due to the approximate rhombic symmetry of the dipolar tensor; a point−dipole model predicts a dipolar tensor of approximate axial symmetry for a terminally bound hydride.[49]

Decomposition of the hydridic ^{1}H coupling constants of **8-H** to the isotropic and dipolar contributions yields an isotropic value of a_{iso} = ±43 MHz and an approximately axial dipolar tensor of **T** = ±[−28, 13, 15] MHz, in good agreement with the predicted tensor symmetry for a terminal hydride. Notably, this experimental a_{iso} value indicates that ±0.030 e$^-$ is localized at the hydride ligand,[50] which is consistent with the DFT-calculated value of −0.029 e$^-$. The greater a_{iso} value observed for **8-H** compared to that of the hydride-bound form of FeMoco correlates with greater spin density localized at the hydrogen atom of **8-H**, presumably due to a greater degree of spin delocalization within the cofactor.

Bimolecular H_2 Elimination from 8-H.

Although Fe^{III}(H)(N_2)(thiolate) **8-H** could be spectroscopically characterized, it is thermally unstable in solution and liberates H_2. Monitoring a THF-d_8 solution of **8-H** at room temperature by ^{1}H NMR spectroscopy reveals the near-quantitative conversion of dark blue 8-H to yellow-brown **6** overnight, which corresponds to formal loss of an H$^\bullet$ and half an N_2 molecule per Fe (Figure 5a). H_2 liberation was confirmed by GC analysis of the headspace.

Monitoring the decay of **8-H** at 50 °C by UV−vis spectroscopy shows that **8-H**, with an absorption at 607 nm, decays in concert with the growth of **6** (Figure 5b). The decay of **8-H** follows second-order kinetics (Figure 5c), consistent with a bimolecular H_2 reductive elimination pathway to allferrous diiron **6**. While we think such a pathway is most plausible, other scenarios, such as a fast monomer−dimer pre-equilibrium with release of H_2 from a dimeric species, could also be consistent with the observed rate dependence on [**8-H**]. The UV−vis timecourse data display isosbestic behavior, and the absence of observable intermediates indicates that transformations prior to the rate determining step are both endergonic and reversible. At 25 °C, the conversion of **8-H** to **6** proceeds with a second-order rate constant of k = 0.068 $M^{-1}\cdot min^{-1}$. Monitoring the decay of **8-D** reveals a kinetic isotope effect of 1.7 at 25 °C, suggesting a role for the hydride ligand in the transition state of the rate-determining step. An early transition state featuring substantial Fe−H character in a bimolecular reductive elimination step is consistent with these data.[51]

Eyring plot analysis of the conversion of **8-H** to diiron **6** provides the following activation parameters: $\Delta H^{\ddagger}$ = 31(4) kcal/mol; $\Delta S^{\ddagger}$ = 39(13) cal/(mol·K); $\Delta G^{\ddagger}$ = 19 kcal/mol (25 °C) (Figure 5d). The large and positive $\Delta S^{\ddagger}$ value is surprising as the transition state of two iron centers interacting in an ordered manner is likely to incur high entropic cost. For comparison, Wayland's classic study of Rh(II)−porphyrin metalloradical M−H/M−R species shows that bimolecular release of R−H provides negative entropies of activation correlated with highly ordered, tertiary transition states (e.g., {[Rh]−H···R−[Rh]}‡).[52]

For the present iron system, we suggest that the large and positive $\Delta S^{\ddagger}$ value may be rationalized if a requisite N_2-dissociation step precedes the rate-determining step via preequilibration of an N_2-bound and an N_2-dissociated state. A plausible mechanism

consistent with this scenario and the data in hand is depicted in Figure 6. Accordingly, an N_2 ligand of **8-H** first dissociates, giving rise to free N_2 and an unobserved, reactive hydride intermediate, $(SiP_2S)Fe^{III}2$ H. This Fe–H intermediate is intercepted by **8-H**, present at much higher concentration, via a transition-state containing one N_2 ligand and two Fe–H subunits, then decaying to H_2 and the final product, diiron **6**. While in principle it may also be possible for two molecules of $(SiP_2S)FeH$ to react directly to form H_2 without a coordinated N_2 ligand in the transition state, we favor the scenario shown in Figure 6.

Thermochemical Parameters for the Fe–H Subunit in 7-H(crown) and 8-H.

The bimolecular elimination of H_2 from **8-H** is indicative of an Fe–H bond with a relatively low homolytic bond strength, consistent with spin density localized on the hydride ligand as evidenced by the large coupling constants to the hydridic ^{1}H nucleus.[27,28] Hence, our use of the term "hydride" masks radical $H^\bullet$ character present in the Fe–H subunit. We therefore sought to explore this idea in greater detail.

The immediate product of $H^\bullet$ loss from **8-H** is the iron(II) species $(SiP_2S)Fe(N_2)$, but this species is not experimentally observed, presumably because the formation of diiron **6** is too facile. However, we have been able to generate and spectroscopically characterize the one- and two-electron reduced relatives of this species, $(SiP_2S)Fe(N_2)^{n-}$ (n = 1, 2, Scheme 2a). Under an N_2 atmosphere, reduction of **6** with excess Na(Hg) in THF followed by addition of 12-crown-4 affords the S = 1/2 iron(I) species $[(SiP_2S)Fe(N_2)][Na(12\text{-crown-}4)_2]$ (9) as a dark red solid ($\nu(N_2)$ = 1963 cm^{-1}). The gas-phase optimized structure of 9 (M06-L: def2tzvp (Fe), def2svp (all other atoms)) indicates less unpaired spin density localized at the sulfur atom (0.02 e^-, 1% overall spin density) than for **8-H** (0.18 e^-, 11% overall spin density). Alternatively, treatment of **6** with excess potassium metal in THF under N_2 provides the dianionic and diamagnetic iron(0) complex $[(SiP_2S)Fe(N_2)][K(THF)_x]_2$ (10) as a dark brown species ($\nu(N_2)$ = 1805 cm^{-1}2). The availability of **9** and **10** provides access to additional data needed to assess the thermochemical properties of the hydride ligand in **8-H**.

Complex **9** shows a reversible $Fe^{II/I}$ redox couple in THF at −1.75 V vs Fc/Fc^+, but data collection in MeCN reveals instead an irreversible oxidation event at −1.71 V vs Fc/Fc^+, presumably due to rapid solvent substitution for the N_2 ligand upon oxidation to produce $(SiP_2S)Fe(MeCN)$, **11** (see below). Additionally, a reversible reductive couple ($Fe^{I/0}$) is observed at −2.94 V vs Fc/Fc^+ in MeCN, corresponding to the conversion of $[(SiP_2S)Fe(N_2)]^{2-}$ to $[(SiP_2S)Fe(N_2)]^{2-}$.

Cyclic voltammograms of the $Fe^{II}(H)(N_2)$(thiolate) **7-H**(**crown**) derivative in MeCN show an irreversible oxidative feature at −0.58 V vs Fc/Fc^+. This feature is significantly shifted from the reversible oxidative $Fe^{III/II}$ couple that is recorded in THF (−1.63 V vs Fc/Fc^+). The irreversibility and extreme solvent dependence of the oxidation potential of **7-H**(**crown**) indicates a process that is more complex than outer-sphere electron transfer may be occurring in MeCN. Thus, for the thermochemical calculations presented below, we have utilized −1.63 V vs Fc/Fc^+ as the value for the **7-H**(**crown**)/**8-H** couple because it is a well-defined, reversible feature as obtained in THF.

Exposing a degassed MeCN-d_3 solution of **7-H(crown)** to an atmosphere of CO_2 results in complete hydride transfer to yield the formate salt [Li(12-crown-4)][HCO_2] and the solvent complex (SiP_2S)Fe(CD_3CN) (**11-*d*$_3$**, Scheme 2b). Defined as the heterolytic dissociation energy of M–H to M^+ and H^- (ΔG_{H^-}),[35,35b] the hydricity of 7-H(crown) in MeCN must therefore be close to, or less than, the hydricity of formate (ΔG_{H^-}= 44 kcal/mol in MeCN).[35b] Loss of H^- from **7-H(crown)** should generate (SiP_2S)Fe(N_2), which is not observed due to facile ligand substitution by MeCN to produce the MeCN adduct **11-*d*$_3$** instead. Thus, the hydricity of **7-H(crown)** can be estimated to have an upper bound of ~44 kcal/mol in MeCN.[53] There are two previous reports of the hydricity of terminally bound Fe-H species.[54,55] A study by our laboratory of a related five-coordinate iron(II) hydride complex, (SiP_3)Fe(H)(H_2), estimated a hydricity of 54.3 ± 0.9 kcal/mol in MeCN,[54] significantly less hydridic than **7-H(crown)**, likely in part reflective of the different charges.

Utilizing available thermodynamic values that relate H^+, $H^\bullet$, and H^- in MeCN (eqs 1 and 2),[35b] the upper bounds for the free energies of $H^+/H^\bullet/H^-$ transfer from 7-**H(crown)** and $H^+/H^\bullet$ transfer from 8-H can be related (Figure 7, eqs 3–6). The approximated upper bounds for homolytic and heterolytic values of Fe–H bond cleavage from **7-H(crown)** and **8-H** are shown in Table 2. Although absolute free energy values for the $H^+/H^\bullet/H^-$ transfers (ΔG) are not established, the difference between any two such free energies ($\Delta\Delta G$) can be determined from eqs 1–6 The Fe–H bond of 7-H(crown) is estimated to have a bond dissociation free energy (BDFE) of <57 kcal/mol and a pK_a of <53. Compared to the Fe–H bond of **7-H(crown)**, the Fe–H bond of **8-H** is considerably more acidic, by more than 22 pK_a units, with an estimated upper bound of pK_a < 30.

$$H^\bullet \rightarrow H^+ + e^- \quad (\Delta G = -53.6\,\text{kcal/mol}) \quad (1)$$

$$H^- \rightarrow H^\bullet + e^- \quad (\Delta G = -26.0\,\text{kcal/mol}) \quad (2)$$

$$\Delta G(\mathbf{7-H}(\text{ crown }))_{H^+} = \Delta G(\mathbf{7-H}(\text{ crown }))_{H^\bullet} - 23.06\left(E_{ox}(\mathbf{10})\right) - 53.6 \quad (3)$$

$$\Delta G(\mathbf{7-H}(\text{crown}))_{H^-} = 23.06\left(E_{ox}(\mathbf{7-H}(\text{crown}))\right) + \Delta G(\mathbf{8-H})_{H^\bullet} + 26.0 \quad (4)$$

$$\Delta G(\mathbf{8-H})_{H^+} = \Delta G(\mathbf{8-H})_{H^\bullet} - 23.06\left(E_{ox}(\mathbf{9})\right) - 53.6 \quad (5)$$

$$\Delta G(\mathbf{7-H}(\text{crown}))_{\text{H}^\bullet} = \Delta G(\mathbf{8-H})_{\text{H}^\bullet} + 23.06\left(E_{\text{ox}}(\mathbf{7-H}(\text{crown})) - E_{\text{ox}}(\mathbf{9})\right) \quad (6)$$

The estimated upper bound for the BDFE of the Fe–H bond in $Fe^{III}(H)(N_2)$(thiolate) 8-**H** of 56 kcal/mol is in close agreement with the DFT-predicted value of 55.6 kcal/mol (M06-L; def2tzvp (Fe), def2svp (all other atoms) in MeCN solvation). It has been previously suggested that M–H bonds with bond dissociation enthalpies of <56 kcal/mol[56] are competent to release H_2 at room temperature (BDFE(H_2) in MeCN = 102.3 kcal/mol).[57] Interestingly, eq 6 indicates that the Fe–H BDFE of Fe(II) **7-H**(**crown**) is only 2.8 kcal/mol greater than that of Fe(III) **8-H** in THF, but **7-H**(crown) is observed to be stable in solution at room temperature, whereas **8-H** undergoes clean conversion to **6** with release of H_2.

Although there is only a small difference in BDFE between the ferrous and ferric hydrides, the K_{eq} for homolytic Fe–H bond cleavage is thus about 100 times greater at room temperature for **8-H** than **7-H**(**crown**); this is further biased by the thermodynamic stability afforded by the formation of 6 rather than $(SiP_2S)FeN_2$, the direct product of Fe–H bond homolysis from **8-H**. Additionally, electrostatic penalties associated with a bimolecular reaction between two anionic species may be a kinetic impediment to H_2 release. Finally, assuming N_2 dissociation would need to precede an H_2 evolution in **7-H**(**crown**), as we have suggested is likely for **8-H** (Figure 6), the stability of 7-**H**(**crown**) may be correlated to a greater kinetic barrier to N_2 dissociation from **7-H**(**crown**), which features a more strongly coordinated N_2 ligand.

CONCLUSION

The synthesis of a trivalent, thiolate–$Fe^{III}(H)(N_2)$ complex has been accomplished and serves as an unusual Fe–N_2 species from the perspective of both oxidation state and the presence of both hydride and thiolate ligands. Its spin is primarily iron-centered, but some leakage onto the thiolate ligand likely contributes to its modest stability. This is the first example of a ferric dinitrogen complex, and it is sufficiently persistent at low temperature to be amenable to characterization by X-ray crystallography and various spectroscopic techniques, including CW EPR and ENDOR spectroscopies. Additionally, we have demonstrated via kinetic measurements that this ferric Fe–H complex undergoes bimolecular reductive elimination to liberate H_2 with a primary kinetic deuterium isotope effect. To the best of our knowledge, this is the first example of a well-defined, bimolecular H_2 elimination process from a terminal Fe–H species. Surprisingly, the entropy of activation for H_2 elimination is positive ($\Delta S^{\ddagger}$ = 39(13) cal/(mol·K)), whereas a large and negative value would be anticipated based solely on the prediction of a highly ordered transition state ([Fe –H···H– Fe]‡). Predissociation of N_2 from thiolate–$Fe^{III}(H)(N_2)$ to afford thiolate–$Fe^{III}(H)$, which is then captured by thiolate– $Fe^{III}(H)(N_2)$ to proceed to an H–H bond-forming transition state, is invoked to accommodate the collective data. Finally, synthetic access to thiolate–$Fe^{II}(H)(N_2)$ and thiolate–$Fe^{III}(H)(N_2)$ species, in addition to the reduced derivatives thiolate–$Fe^{I}(N_2)^{-}$ and thiolate–$Fe^{0}(N_2)^{2-}$, has provided access to the physical detail needed

to estimate important thermochemical H^+, $H^\bullet$, and H^- parameters of broad current interest, and within an $S = 1/2$ Fe system that evolves H_2.

Supplementary Material

Refer to Web version on PubMed Central for supplementary material.

ACKNOWLEDGMENTS

The authors are grateful to the NIH for support via Grant No. GM-070757 and to the National Science Foundation for support of the Caltech EPR Facility via Grant No. NSF-153194. N.X.G. acknowledges an NSF Graduate Research Fellowship. Dr. Gaël Ung provided technical assistance toward the synthesis of 2 and 3. Dr. Michael Takase and Larry Henling are thanked for providing crystallographic assistance. We thank Dr. Jay Winkler for helpful discussions.

REFERENCES

(1). For select examples, see:Yandulov DV; Schrock RR Science 2003, 301, 76–78. [PubMed: 12843387] Arashiba K; Miyake Y; Nishibayashi Y Nat. Chem 2011, 3, 120–125. [PubMed: 21258384] Anderson JS; Rittle J; Peters JC Nature 2013, 501, 84–87. [PubMed: 24005414] Stucke N; Floeser B; Weyrich T; Tuczek F Eur. J. Inorg. Chem 2018, 2018, 1337–1355.

(2). Buscagan TM; Oyala PH; Peters JC Angew. Chem., Int. Ed 2017, 56, 6921–6926.

(3). Rees DC; Howard JB Curr. Opin. Chem. Biol 2000, 4, 559–566. [PubMed: 11006545]

(4). Hoffman BM; Lukoyanov D; Yang Z-Y; Dean DR; Seefeldt LC Chem. Rev 2014, 114, 4041–4062. [PubMed: 24467365]

(5). Einsle O; Tezcan FA; Andrade SLA; Schmid B; Yoshida M; Howard JB; Rees DC Science 2002, 297, 1696–1700. [PubMed: 12215645]

(6). Lough S; Burns A; Watt GD Biochemistry 1983, 22, 4062–4066.

(7). Doan PE; Telser J; Barney BM; Igarashi RY; Dean DR; Seefeldt LC; Hoffman BM J. Am. Chem. Soc 2011, 133, 17329–17340. [PubMed: 21980917]

(8). Morrison CN; Spatzal T; Rees DC J. Am. Chem. Soc 2017, 139, 10856–10862. [PubMed: 28692802]

(9). (a)Igarashi RY; Laryukhin M; Dos Santos PC; Lee H-I; Dean DR; Seefeldt LC; Hoffman BM J. Am. Chem. Soc 2005, 127, 6231–6241. [PubMed: 15853328] (b)Lukoyanov DA; Khadka N; Yang Z-Y; Dean DR; Seefeldt LC; Hoffman BM Inorg. Chem 2018, DOI: 10.1021/acs.inorgchem.8b00271.

(10). Rittle J; McCrory CCL; Peters JC J. Am. Chem. Soc 2014, 136, 13853–13862. [PubMed: 25184795]

(11). Bart SC; Lobkovsky E; Bill E; Wieghardt K; Chirik PJ Inorg. Chem 2007, 46, 7055–7063. [PubMed: 17655227]

(12). Takaoka A; Mankad NP; Peters JC J. Am. Chem. Soc 2011, 133, 8440–8443. [PubMed: 21574618]

(13). Creutz SE; Peters JC J. Am. Chem. Soc 2015, 137, 7310–7313. [PubMed: 26039253]

(14). Čorić, I; Mercado BQ; Bill E; Vinyard DJ; Holland PL Nature 2015, 526, 96–99. [PubMed: 26416755]

(15). (a)Čorić I; Holland PL J. Am. Chem. Soc 2016, 138, 7200–7211. [PubMed: 27171599] (b)Speelman AL; Holland PL In Nitrogen Fixation; Nishibayashi Y, Ed.; Springer International Publishing: Cham, 2017; pp 197–213.

(16). Lukoyanov D; Barney BM; Dean DR; Seefeldt LC; Hoffman BM Proc. Natl. Acad. Sci. U. S. A 2007, 104, 1451–1455. [PubMed: 17251348]

(17). Simpson FB; Burris RH Science 1984, 224, 1095–1097. [PubMed: 6585956]

(18). Lubitz W; Ogata H; Rüdiger O; Reijerse E Chem. Rev 2014, 114, 4081–4148. [PubMed: 24655035]

(19). Schilter D; Camara JM; Huynh MT; Hammes-Schiffer S; Rauchfuss TB Chem. Rev 2016, 116, 8693–8749. [PubMed: 27353631]

(20). (a)Kaeffer N; Chavarot-Kerlidou M; Artero V Acc. Chem. Res 2015, 48, 1286–1295. [PubMed: 25941953] (b)DuBois DL; Bullock MR Eur. J. Inorg. Chem 2011, 2011, 1017–1027.(c)Dempsey JL; Brunschwig BS; Winkler JR; Gray HB Acc. Chem. Res 2009, 42, 1995–2004. [PubMed: 19928840]

(21). Du P; Eisenberg R Energy Environ. Sci 2012, 5, 6012–6021.

(22). (a)Hu X; Brunschwig BS; Peters JC J. Am. Chem. Soc 2007, 129, 8988–8998. [PubMed: 17602556] (b)Marinescu SC; Winkler JR; Gray HB Proc. Natl. Acad. Sci. U. S. A 2012, 109, 15127–15131. [PubMed: 22949704] (c)Rose MJ; Gray HB; Winkler JR J. Am. Chem. Soc 2012, 134, 8310–8313. [PubMed: 22583071]

(23). Besora M; Lledós A; Maseras F Chem. Soc. Rev 2009, 38, 957–966. [PubMed: 19421574]

(24). Bullock RM; Appel AM; Helm ML Chem. Commun 2014, 50, 3125–3143.

(25). (a)Packett DL; Trogler WC Inorg. Chem 1988, 27, 1768–1755.(b)Chirik PJ; Henling LM; Bercaw JE Organometallics 2001, 20, 534–544.(c)Kaesz HD; Saillant RB Chem. Rev 1972, 72, 231–281.(d)Daida EJ; Peters JC Inorg. Chem 2004, 43, 7474–7485. [PubMed: 15530098] (e)Deutsch PP; Eisenberg R Organometallics 1990, 9, 709–718.

(26). (a)Collman JP; Wagenknecht PS; Lewis NS J. Am. Chem. Soc 1992, 114, 5665–5673. (b)Collman JP; Hutchison JE; Wagenknecht PS; Lewis NS; Lopez MA; Guilard RJ Am. Chem. Soc 1990, 112, 8206–8208.(c)Norton JR Acc. Chem. Res 1979, 12, 139–145.(d)Evans J; Norton JR J. Am. Chem. Soc 1974, 96, 7577–7578.(e)Inoki D; Matsumoto T; Nakai H; Ogo S Organometallics 2012, 31, 2996–3001.

(27). (a)Hu Y; Shaw AP; Estes DP; Norton JR Chem. Rev 2016, 116, 8427–8462. [PubMed: 26828562] (b)Poli R, Paramagnetic Mono-and Polyhydrides of the Transition Metals In Recent Advances in Hydride Chemistry; Poli R, Peruzzini M, Eds.; Elsevier: Eastbourne, 2001; pp 139–188.

(28). (a)Chiang KP; Scarborough CC; Horitani M; Lees NS; Ding K; Dugan TR; Brennessel WW; Bill E; Hoffman BM; Holland PL Angew. Chem., Int. Ed 2012, 51, 3658–3662.(b)Hamon P; Toupet L; Hamon J-R; Lapinte C Organometallics 1992, 11, 1429–1431.(c)Hamon P; Hamon J-R; Lapinte CJ Chem. Soc., Chem. Commun 1992, 1602–1603.

(29). Crossland JL; Tyler DR Coord. Chem. Rev 2010, 254, 1883–1894.

(30). For studies of heterobimetallic bimolecular HER, see:Mazzacano TJ; Mankad NP J. Am. Chem. Soc 2013, 135, 17258–17261. [PubMed: 24074248] Parmelee SR; Mazzacano TJ; Zhu Y; Mankad NP; Keith JA ACS Catal. 2015, 5, 3689–3699.

(31). Koelle U; Ohst S Inorg. Chem 1986, 25, 2689–2694.

(32). For related examples of unimolecular reductive elimination from multimetallic, first-row transition-metal hydride complexes, see:Vollhardt KPC; Cammack JK; Matzger AJ; Bauer A; Capps KB; Hoff CD Inorg. Chem 1999, 38, 2624–2631.Lee Y; Anderton KJ; Sloane FT; Ermert DM; Abboud KA; García-Serres R; Murray LJ J. Am. Chem. Soc 2015, 137, 10610–10617. [PubMed: 26270596] Manz D-H; Duan P-C; Dechert S; Demeshko S; Oswald R; John M; Mata RA; Meyer FJ Am. Chem. Soc 2017, 139, 16720–16731.Bellows SM; Arnet NA; Gurubasavaraj PM; Brennessel WW; Eckhard B; Cundari TR; Holland PL J. Am. Chem. Soc 2016, 138, 12112–12123. [PubMed: 27598037] Yu Y; Sadique AR; Smith JR; Dugan TR; Cowley RE; Brennessel WW; Flaschenriem CJ; Bill E; Cundari TR; Holland PL J. Am. Chem. Soc 2008, 130, 6624–6638. [PubMed: 18444648] Ding K; Brennessel WW; Holland PL J. Am. Chem. Soc 2009, 131, 10804–10805. [PubMed: 19621923]

(33). The elimination of H2 from two M–H species (2M–H → H2 + M2) may also occur through an M–M-bonded species, whereby the intermediate prior to reductive elimination is a dinuclear M2H2 species; see:Halpern J; Pribaníc M Inorg. Chem 1970, 9, 2616–2618.Ungváry F; Markó LJ Organomet. Chem 1969, 20, 205–209.Trinquier G; Hoffmann R Organometallics 1984, 3, 370–380.

(34). It has been reported that CpFe(CO)2H (FpH) undergoes reductive elimination of H2 to yield {CpFe(CO)2}2. See:Green MLH; Street CN; Wilkinson GZ Naturforsch., B: J. Chem. Sci 1959, 14, 738.However, subsequent studies provided evidence to suggest that the H2 evolution was catalyzed by the presence of a trace oxidant. See:Shackleton TA; Mackie SC; Fergusson SB;

Johnston LJ; Baird MC Organometallics 1990, 9, 2248–2253.The reverse bimolecular oxidative addition of H2 (Fp2 + H2 → 2 FpH) is known to occur at high pressures of H2 (Fp2 + H2 → 2 FpH). See:Chang B-H; Coil PC; Brown MJ; Barnett KW J. Organomet. Chem 1984, 270, C23–C25.

(35). (a)Waldie KM; Ostericher AL; Reineke MH; Sasayama AF; Kubiak CP ACS Catal. 2018, 8, 1313–1324.(b)Wiedner ES; Chambers MB; Pitman CL; Bullock RM; Miller AJM; Appel AM Chem. Rev 2016, 116, 8655–8692. [PubMed: 27483171] (c)Pearson RG Chem. Rev 1985, 85, 41–49.

(36). (a)Whited MT; Mankad NP; Lee Y; Oblad PF; Peters JC Inorg. Chem 2009, 48, 2507–2517. [PubMed: 19209938] (b)Lee Y; Mankad NP; Peters JC Nat. Chem 2010, 2, 558–565. [PubMed: 20571574]

(37). McGinley PL; Koh JT J. Am. Chem. Soc 2007, 129, 3822–3823. [PubMed: 17348658]

(38). Del Castillo TJ; Thompson NB; Peters JC J. Am. Chem. Soc 2016, 138, 5341–5350. [PubMed: 27026402]

(39). Hendrich MP; Gunderson W; Behan RK; Green MT; Mehn MP; Betley TA; Lu CC; Peters JC Proc. Natl. Acad. Sci. U. S. A 2006, 103, 17107–17112. [PubMed: 17090681]

(40). Stoian SA; Vela J; Smith JM; Sadique AR; Holland PL; Münck E; Bominaar EL J. Am. Chem. Soc 2006, 128, 10181–10192. [PubMed: 16881648]

(41). For a related example of multiple N2 stretches arising from variable cation interactions, see:Moret M-E; Peters J Angew. Chem., Int. Ed 2011, 50, 2063–2067.

(42). Fryzuk MD; Johnson SA Coord. Chem. Rev 2000, 200, 379.

(43). (a)Jenkins DM; Peters JC J. Am. Chem. Soc 2005, 127, 7148–7165. [PubMed: 15884957] (b)Creutz SE; Peters JC Inorg. Chem 2016, 55, 3894–3906. [PubMed: 27042863]

(44). An asymmetric 57Fe Mössbauer spectrum has been similarly observed for (i) [Fe(Cp*)(dppe)(CO)(H)]PF6, an S = 1/2 Fe(III) hydride. See ref 28c. (ii) Polyphosphine-bound iron complexes have been studied previously by our lab. See, for example:Rittle J; Peters JC J. Am. Chem. Soc 2016, 138, 4243–4248. [PubMed: 26937584]

(45). Unless otherwise noted, [Cp*2Fe][PF6] was utilized as the oxidant to prepare EPR and ENDOR samples of 8-H and 8-D. Decamethylferrocenium was favored over cobaltocenium because the resultant Cp*2Fe byproduct is diamagnetic. However, the 77 K X-band EPR spectrum obtained via oxidation with [Cp2Co][PF6] was indiscernible from that obtained utilizing [Cp*2Fe][PF6] as the oxidant (see the SI for complete details).

(46). (a)Chang Y-H; Su C-L; Wu R-R; Liao J-H; Liu Y-H; Hsu H-FJ Am. Chem. Soc 2011, 133, 5708–5711.(b)Broering EP; Dillon S; Gale EM; Steiner RA; Telser J; Brunold TC; Harrop TC Inorg. Chem 2015, 54, 3815–3828. [PubMed: 25835183]

(47). The gas-phase DFT-optimized structure of 8-H is calculated to have an N2 stretch of 2208 cm−1 and an Fe−H stretch of 1907 cm−1.

(48). Lukoyanov D; Khadka N; Yang Z-Y; Dean DR; Seefeldt LC; Hoffman BM J. Am. Chem. Soc 2016, 138, 10674–10683. [PubMed: 27529724]

(49). Kinney RA; Saouma CT; Peters JC; Hoffman BM J. Am. Chem. Soc 2012, 134, 12637–12647. [PubMed: 22823933]

(50). The spin density at the hydride ligand is calculated using the aiso value for a free hydrogen atom of 1420 MHz; see:Wittke JP; Dicke RH Phys. Rev 1956, 103, 620–631.

(51). Gomez-Gallego M; Sierra MA Chem. Rev 2011, 111, 4857–4963. [PubMed: 21545118]

(52). Wayland BB; Ba S; Sherry AE J. Am. Chem. Soc 1991, 113, 5305–5311.

(53). Following the reaction of 7-H(crown) with CO by 1 2 H NMR reveals direct conversion of 7-H(crown) to 11; a N2-bound intermediate is not observed in the reaction mixture. It may be possible that the thermodynamic stability afforded by MeCN coordination drives the hydride transfer reaction forward, even if the hydricity of 7-H(crown) is slightly greater than 44 kcal/mol. Thus, 44 kcal/mol is determined to be an approximate upper bound for the hydricity of 7-H(crown).

(54). Fong H; Peters JC Inorg. Chem 2015, 54, 5124–5135. [PubMed: 25549663]

(55). Estes DP; Vannucci AK; Hall AR; Lichtenberger DL; Norton JR Organometallics 2011, 30, 3444–3447.

(56). Kiss G; Zhang K; Mukerjee SL; Hoff CD J. Am. Chem. Soc 1990, 112, 5657–5658.
(57). Warren JJ; Tronic TA; Mayer JM Chem. Rev 2010, 110, 6961–7001. [PubMed: 20925411]

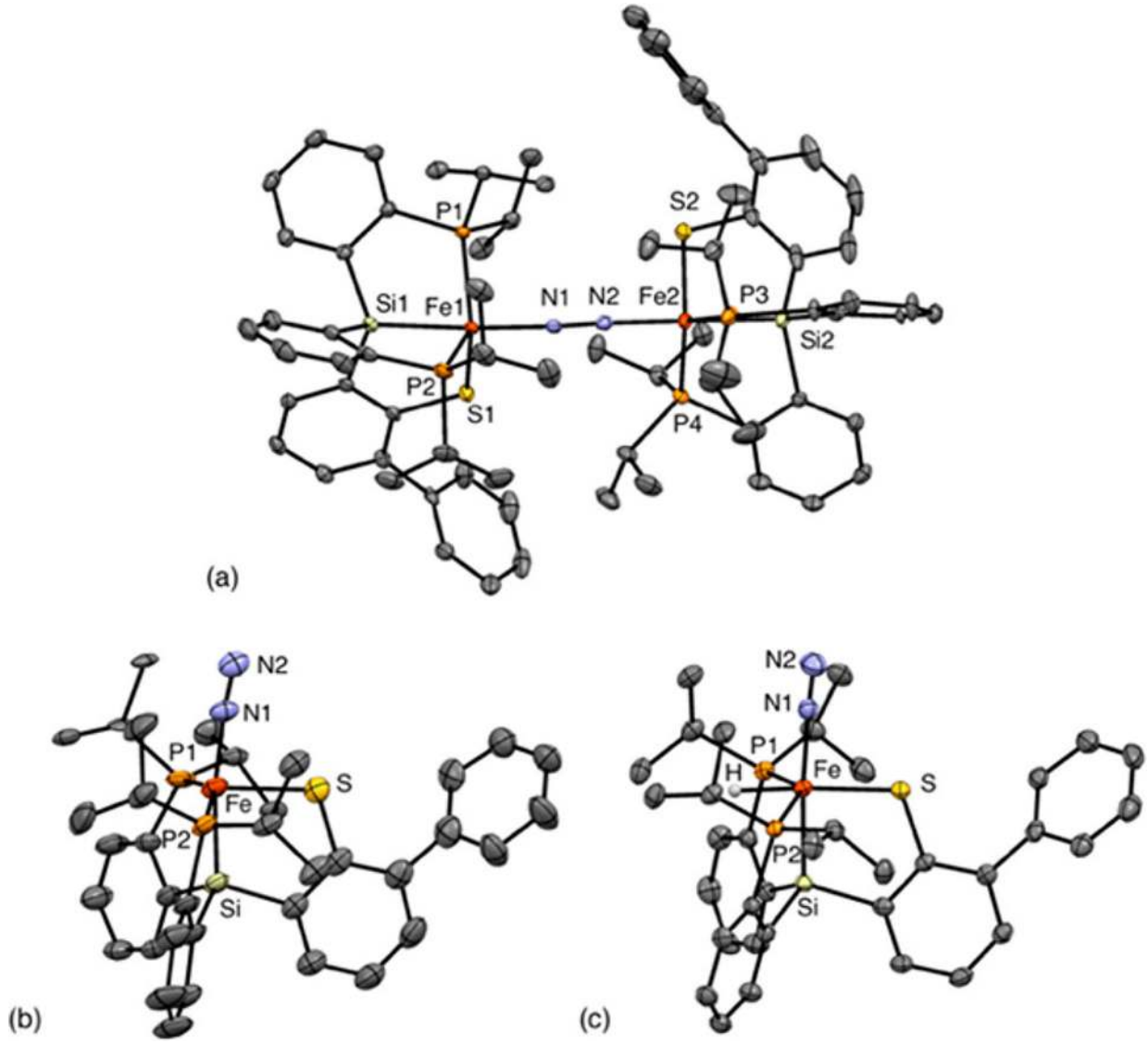

Figure 1.

X-ray structures of (a) **6**, (b) **7**-**H**(**crown**), and (c) **8**-**H**. C-*H* hydrogen atoms, solvent molecules, and the counterion of **7**-**H**(**crown**) are omitted for clarity. Ellipsoids are depicted at 50% occupancy.

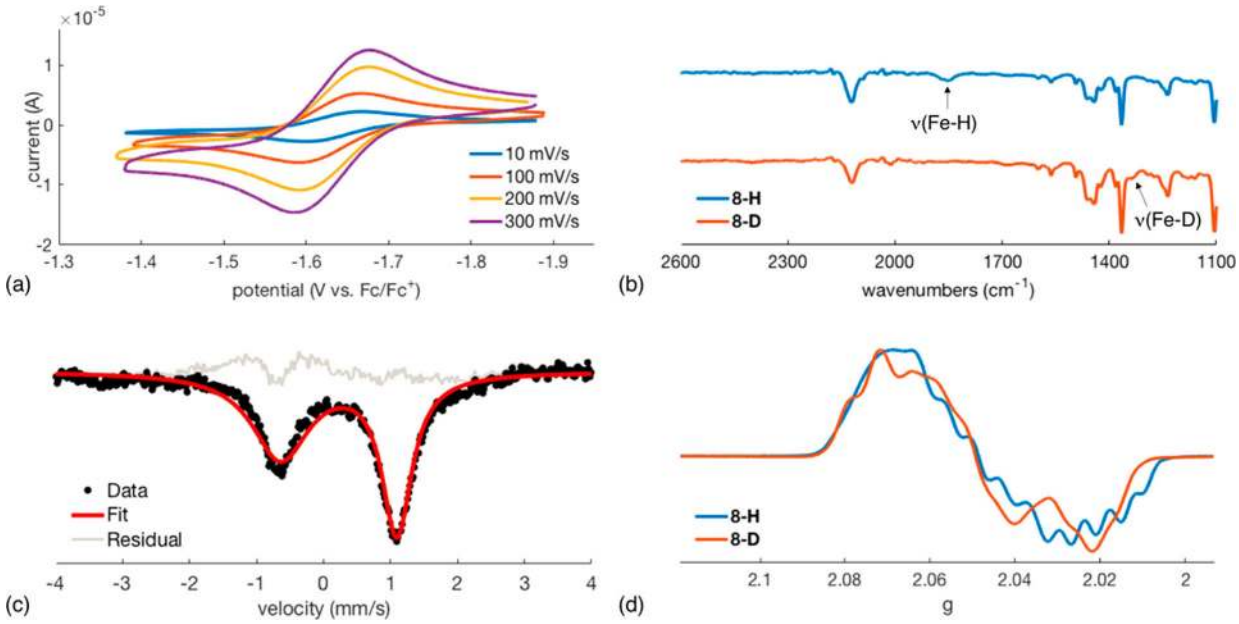

Figure 2.

(a) Cyclic voltammetry of **7-H** at various scan rates depicting the $Fe^{III/II}$ couple at −1.63 V vs Fc/Fc^+ (0.4 M $[NBu_4][PF_6]$ in THF). (b)Thin-film IR spectra of isotopologues **8-H** and **8-D**. (c) ^{57}Fe Mössbauer spectrum of **8-H** collected at 80 K with a 50 mT applied parallel field. (d) 77 K CW X-band EPR spectra of isotopologues **8-H** and **8-D** in 2-MeTHF.

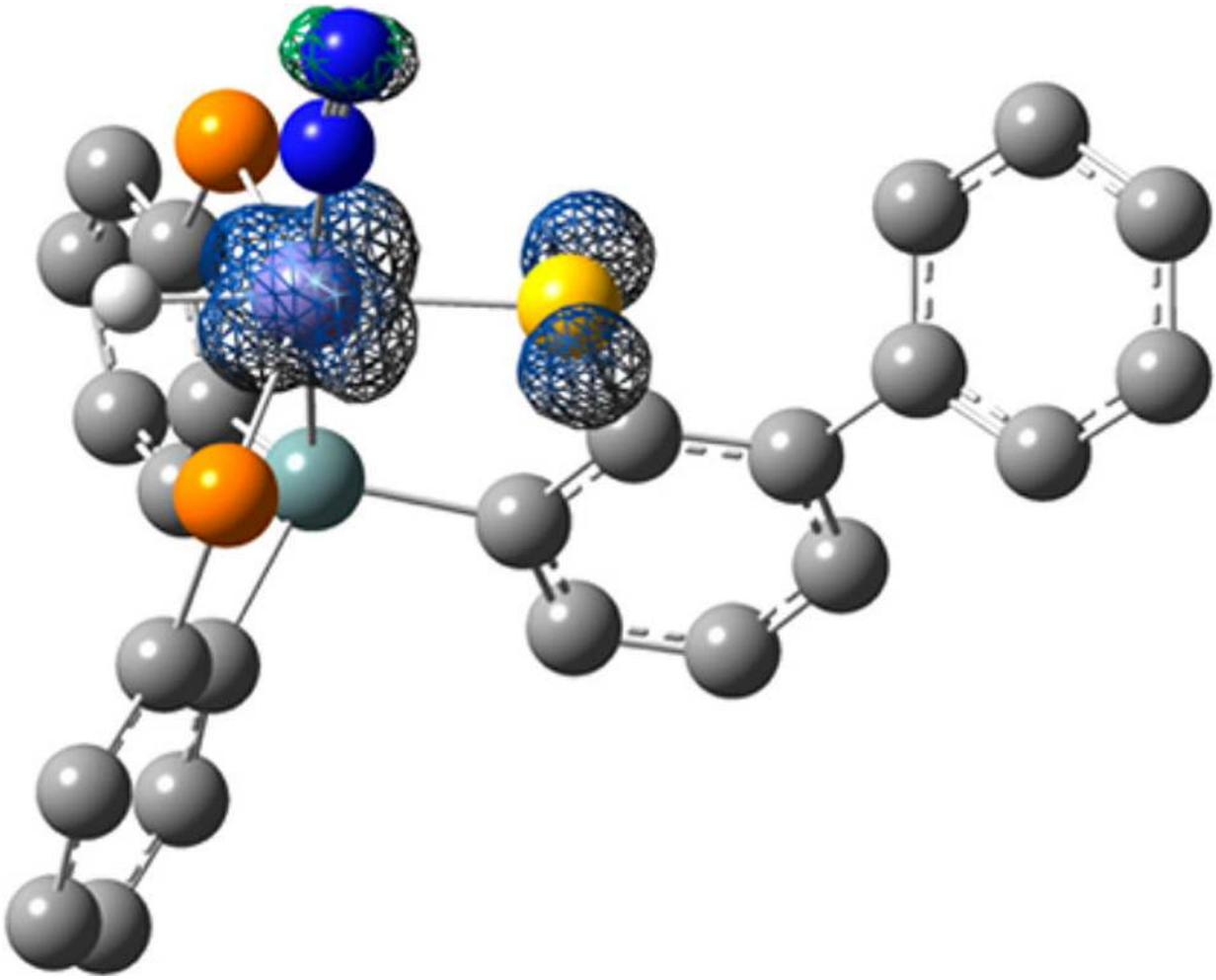

Figure 3.

Spin density map of gas-phase optimized structure of compound **8-H** (isovalue: 0.005 e-/Å^3; M06-L functional: def2tzvp (Fe), def2svp (all other atoms)). Atom colors: Fe (purple), S (yellow), H (white), P (orange), C (gray), N (blue), Si (light blue).

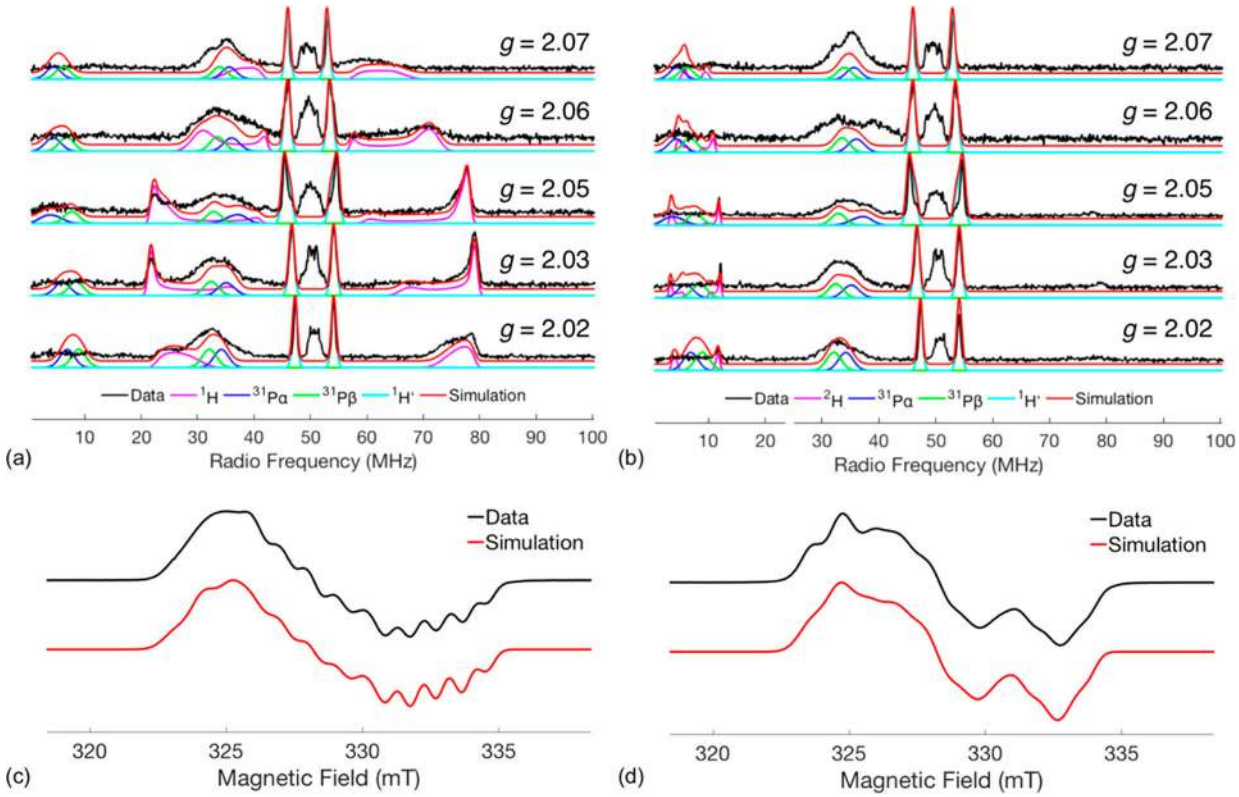

Figure 4.

Field-dependent Q-band Davies ENDOR of (a) **8-H** and (b) **8-D** in 2-MeTHF with simulations. Simulation parameters: **g** = [2.07, 2.0475, 2.02]; **A**(^{31}Pα) = ± [31, 36, 27] MHz; **A**(^{31}Pβ) = ± [28, 25, 23] MHz; **A**(^{1}H') = ± [6.8, 10, 6.8] MHz. Figure 4a was simulated with additional coupling to Fe-*H* (**A**(^{1}H) = ± [15, 56, 58] MHz), whereas Figure 4b was simulated with additional coupling to Fe-*D* (**A**(^{2}H) = ± [2.3, 8.6, 8.9] MHz). Summation of individual component ENDOR simulations is displayed in red. Experimental conditions: microwave frequency = 33.674 GHz; MW π pulse length = 40 ns; interpulse delay τ = 300 ns; π_{RF} pulse length = 15 μs; TRF delay = 1 μs; shot repetition time (srt) = 5 ms; temperature = 18.5 K; RF frequency randomly sampled. 77 K X-band CW EPR spectra of (c) **8-H** and (d) **8-D** in 2-MeTHF with simulations. The CW EPR spectra were simulated with the same parameters as the corresponding ENDOR spectra.

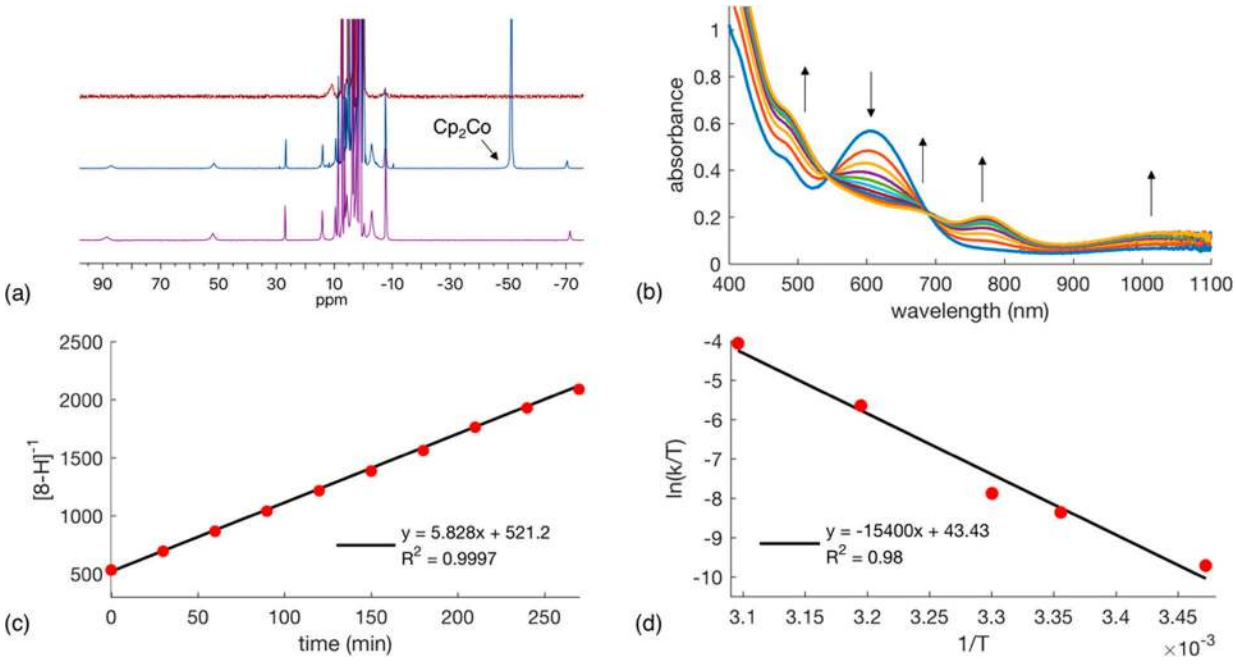

Figure 5.

(a) ^{1}H NMR spectra of **8-H** in THF-d_8 collected at −78 °C (top) and after stirring at 25 °C overnight (middle) with an ^{1}H NMR spectrum of **6** in THF-d_8 (bottom). (b) UV−vis spectra showing the decay of **8-H** and the growth of **6** at 50 °C. Spectra were collected every 30 min. (c) Plot of $[\mathbf{8\text{-}H}]^{-1}$ (M^{-1}) versus time using the UV−vis data shown in Figure 5b. (d) Eyring plot of the conversion of **8-H** to **6** (T in K, k in $M^{-1}\cdot min^{-1}$).

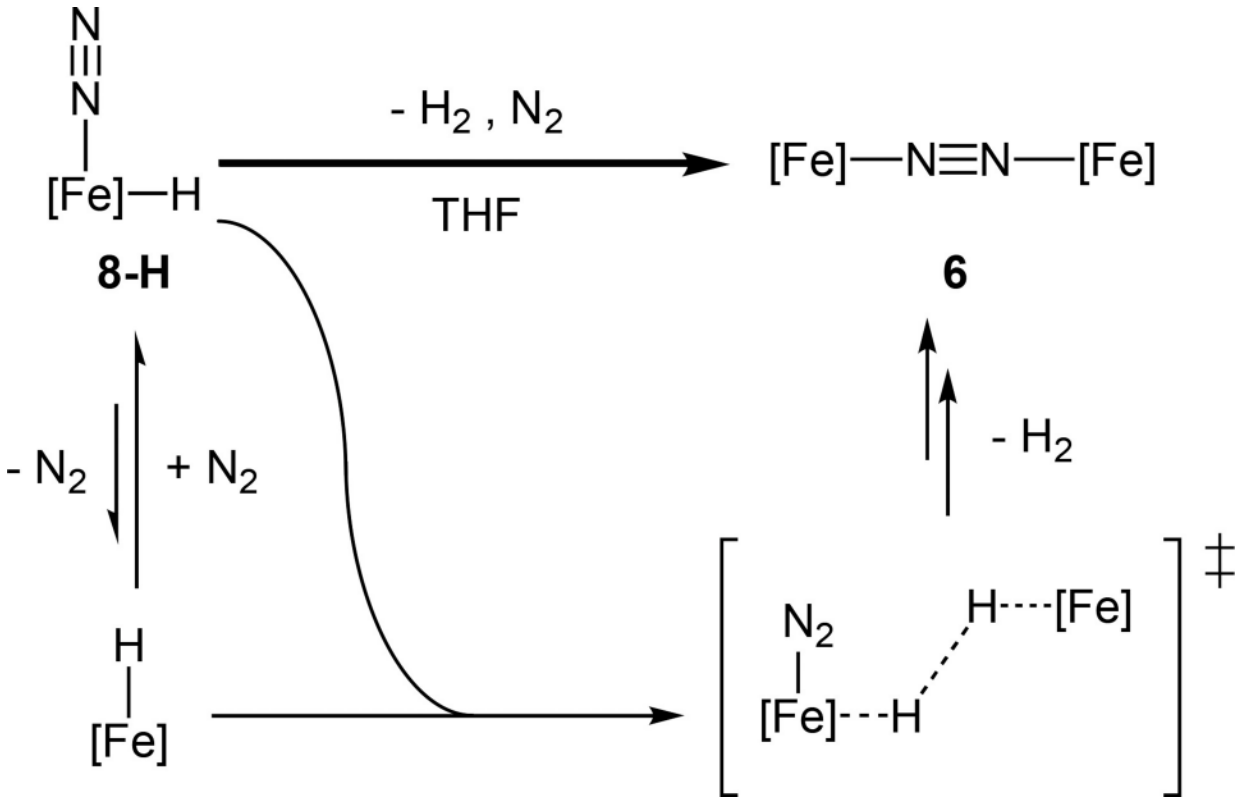

Figure 6.
Proposed pathway for the conversion of **8-H** to **6**, where [Fe] = (SiP_2S)Fe.

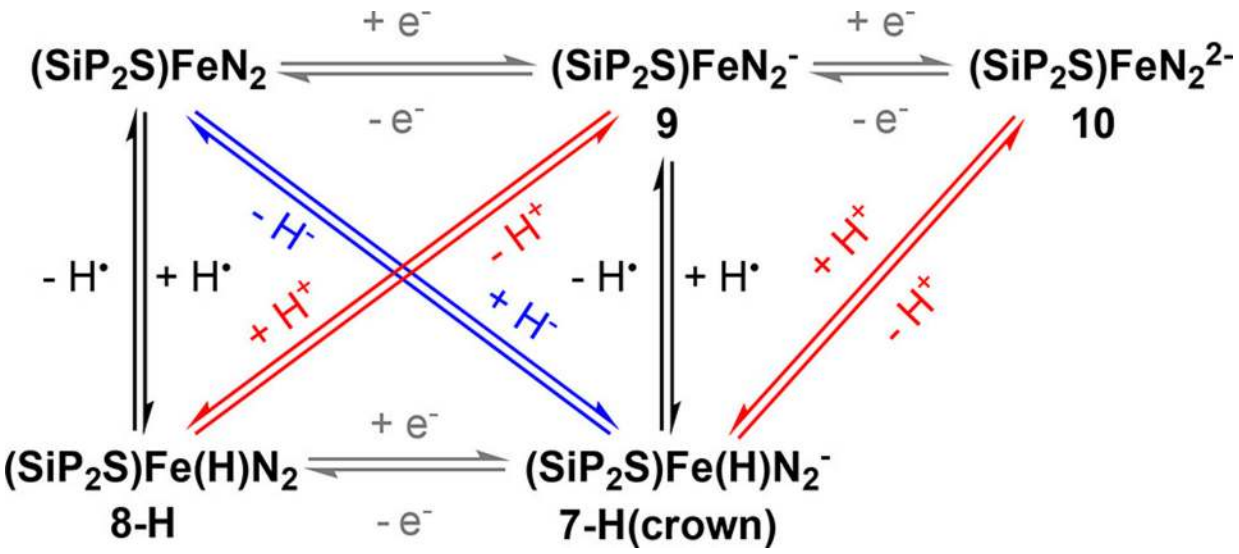

Figure 7.

Thermochemical scheme relating H^+, $H^\bullet$, and H^- transfers from **7-H**(**crown**) and **8-H**.

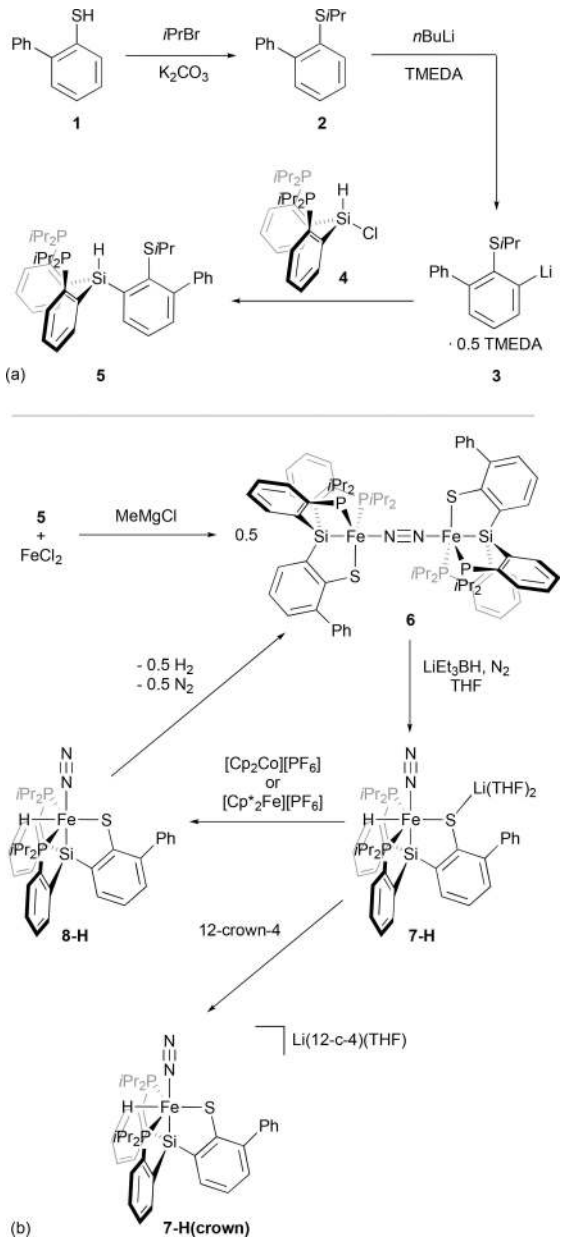

Scheme 1.

(a) Synthesis of Ligand Precursor 5 (b) Metalation Procedure of 5 To Yield Diiron 6 and the Synthesis of Species 7-H, 7-H(crown), and 8-H

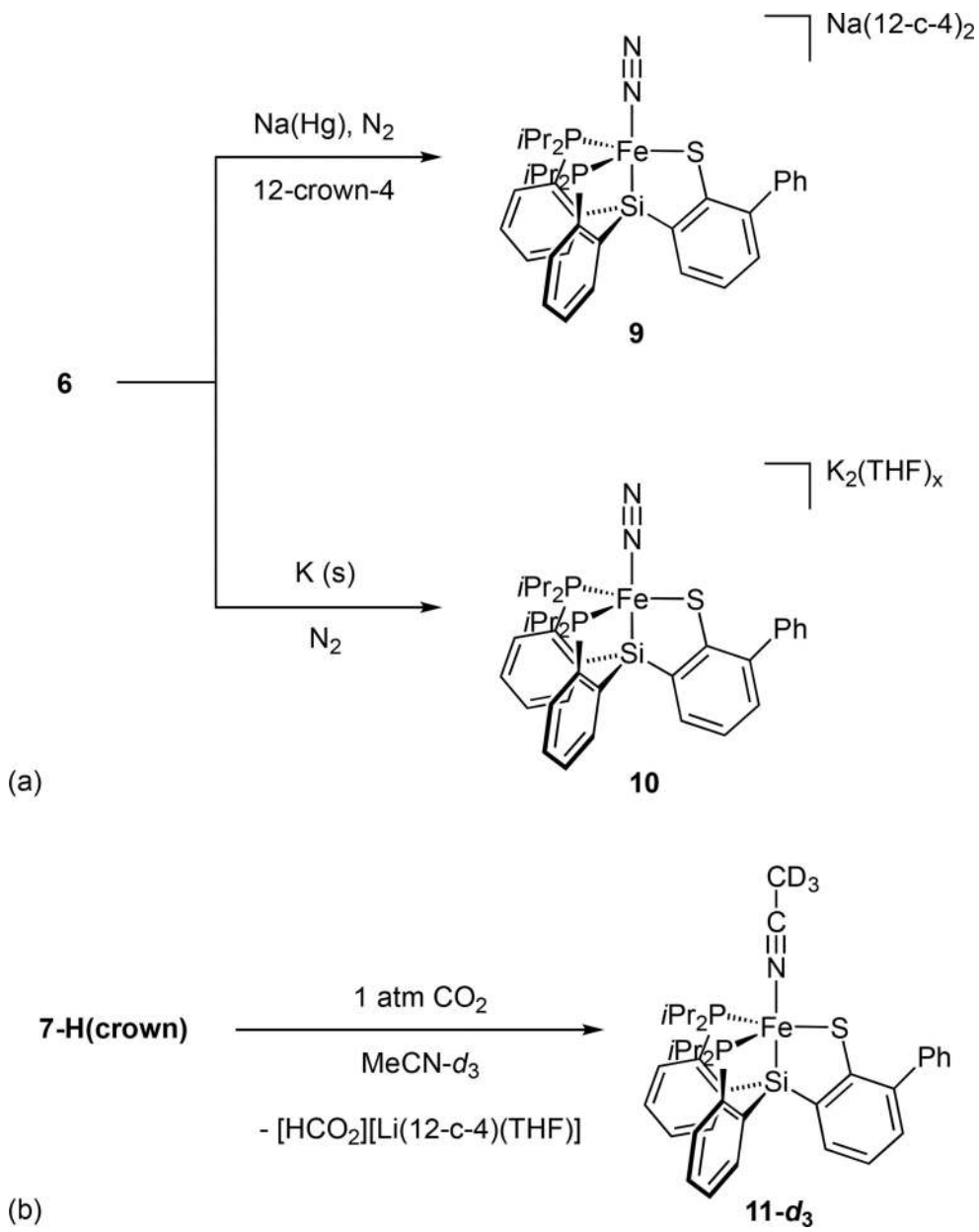

Scheme 2.

(a) Synthesis of 9 and 10 via Reduction of 6 (b) Hydride Transfer upon Treatment of 7-H(crown) with CO2

Table 1.

Select Bond Metrics and Angles of Complexes 6, 7-H(crown), and 8[a]

	d(Fe–N)	*d*(N–N)	*d*(Fe–P)	*d*(Fe–S)	*d*(Fe–H)	∠(P-Fe-P)	∠(P-Fe-S)
6	1.871(1)	1.138(2)	2.3059(6)	2.2314(5)		130.72(2)	110.53(2)
			2.3132(7)				112.59(2)
	1.865(1)		2.3444(6)	2.2323(6)		131.34(2)	110.75(2)
			2.3189(5)				111.98(2)
7-H(crown)	1.810(4)	1.117(6)	2.16(1)	2.339(2)		146.5(3)	104.21(6)
			2.180(2)				106.3(3)
8-H	1.882(3)	1.077(4)	2.2541(8)	2.2185(7)	1.54(4)	138.70(3)	106.98(3)
			2.2422(8)				111.19(3)

[a]Bond distances are listed in Å and bond angles in degrees.

Table 2.

Oxidation Potentials and Thermochemical Parameters Pertaining to Fe–H Bond Cleavage of 7-H(crown) and 8-H

	hydricity[a]	BDFE[a]	pK_a	E_{ox}[b]
7-H(crown)	<44	<57	<53	−1.63
8-H		<56	<30	
9				−1.71
10				−2.94

[a] Values in kcal/mol.

[b] Potentials reported in V vs Fc/Fc^+